THE JOURNAL OF PHYSICAL CHEMISTRY B

Article

pubs.acs.org/JPCB

Molecular Dynamics Studies of Fluid/Oil Interfaces for Improved Oil Recovery Processes

Lucas S. de Lara, Mateus F. Michelon, and Caetano R. Miranda*

Centro de Ciências Naturais e Humanas (CCNH), Universidade Federal do ABC (UFABC) Santo André, SP, Brazil

ABSTRACT: In our paper, we study the interface wettability, diffusivity, and molecular orientation between crude oil and different fluids for applications in improved oil recovery (IOR) processes through atomistic molecular dynamics (MD). The salt concentration, temperature, and pressure effects on the physical chemistry properties of different interfaces between IOR agents [brine (H_2O + % NaCl), CO_2, N_2, and CH_4] and crude oil have been determined. From the interfacial density profiles, an accumulation of aromatic molecules near the interface has been observed. In the case of brine interfaced with crude oil, our calculations indicate an increase in the interfacial tension with increasing pressure and salt concentration, which favors oil displacement. On the other hand, with the other fluids studied (CO_2, N_2, and CH_4), the interfacial tension decreases with increasing pressure and temperature. With interfacial tension reduction, an increase in fluid diffusivity in the oil phase is observed. We also studied the molecular orientation properties of the hydrocarbon and fluids molecules in the interface region. We perceived that the molecular orientation could be affected by changes in the interfacial tension and diffusivity of the molecules in the interface region with the increased pressure and temperature: pressure (increasing) → interfacial tension (decreasing) → diffusion (increasing) → molecular ordering. From a molecular point of view, the combination of low interfacial tension and high diffusion of molecules in the oil phase gives the CO_2 molecules unique properties as an IOR fluid compared with other fluids studied here.

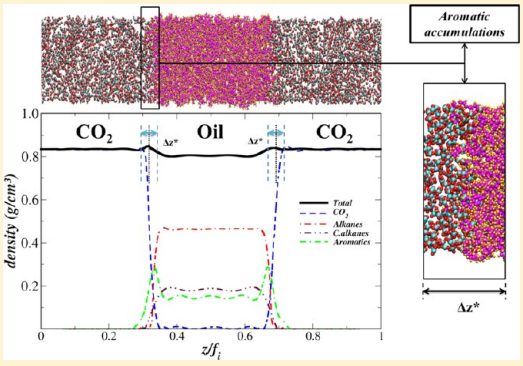

1. INTRODUCTION

Improved oil recovery (IOR) techniques are currently of great strategic importance because the yield of oil wells, with current extraction techniques, is of about 50% of the oil contained in the well. There are various IOR techniques, including injection of gas and chemicals.[1] Currently, the main strategy is to reduce the interfacial tension (IFT) or the viscosity of crude oil by molecular additives, which can be adsorbed on the oil−fluid interface or migrate to the crude oil through the interface. Although the experimental measurements of the wettability at nanoscale under reservoir conditions of temperature and pressure are still quite challenging, molecular simulations can provide an efficient and reliable way to determine these properties and understand the underlying molecular mechanism involved in the fluid−oil interfaces.[2−4]

Interfaces between two immiscible fluids play an important role in many natural and technological processes.[5−9] Experimental measurements for liquid−liquid and liquid−gas interfaces are challenging,[10−15] particularly for confined fluids and high pressure. This is because of its relatively small size interface, usually only a few nanometers in width.

In oil recovery process, fluids can be injected into oil reservoirs for different reasons, such as either to maintain the reservoir pressure or to improve oil recovery. Fluids can be injected into the dome above the oil zone, dissolves in the oil, thus lowering its density, interfacial tension, and viscosity. These changes may be favorable to induce the repressuring of the oil reservoir when the fluid injection may be dissolved under different conditions prevailing at high rates. Water flooding is the most usual method applied in a reservoir because of its availability and easy manipulation compared with other available IOR techniques. The water injected into the reservoir can have different origins, including subterranean aquifers. Therefore, the degree of salinity concentration in brine can have an influence on the process, and it should be explicitly described.

Also in this context, a miscible displacement of hydrocarbons can be obtained through the dissolution of the CO_2 into the oil phase, for example. Because of that, the injection of CO_2 has been used for IOR over decades with significant success.[16,17] CO_2 is known to be highly soluble in oil. The CO_2 dissolution can not only increase oil saturation above the residual saturation but also reduce the oil viscosity, which leads to oil flow with better mobility.[17] At sufficiently high density, above the minimal miscible pressure (MMP) between the CO_2 and the oil, CO_2 is able to not only displace oil, but also to maintain the pressure through the recovery process with a relatively high oil recovery. In a typical reservoir with multicomponent crude oil, the CO_2/crude oil MMP is a complex function, which may change with temperature, reservoir depth, and crude oil composition. Experimentally, a simplified situation can be set up to study CO_2/crude oil miscibility and displacement at

Received: October 15, 2012
Revised: November 15, 2012
Published: November 19, 2012

constant temperature and pressure in core samples at different wettabilities and initial saturations.[18]

Other possibilities for fluid injection are either natural gas (mainly methane) or nitrogen; both are largely available in the reservoirs. Gaseous nitrogen N_2 injection techniques can also contribute to increasing the reservoir pressure and mobilizing the oil. Nitrogen is attractive for injection into reservoirs because it is inert and noncorrosive and it can be manufactured on-site at less cost once it can be extracted from air by cryogenic separation. In general, when nitrogen is injected into a reservoir, it forms a miscible front by displacing lighter components from the oil. The combined gas front becomes even more enriched until the point that it can be miscible within the oil phase. Continued injection of nitrogen pushes the miscible front through the reservoir, moving the displaced oil toward production wells. H_2O can be injected alternately with the nitrogen to increase the sweep efficiency and oil recovery. On the other hand, the use of methane serves primarily for the maintenance of pressure in the reservoir. Its uses in the injection process are based on the fact that it can easily interact with hydrocarbon molecules and diffuse within the oil phase.

In this work, we study through classical molecular dynamics simulations, the density profile, interfacial tensions, diffusion coefficients, and structural information for molecules in interface systems, under typical conditions of pressures and temperatures found in reservoirs. We address four fluids typically used in the oil and gas industry: H_2O (brine), CO_2, N_2, CH_4 and a crude oil model. The understanding of physical and chemical processes taking place at the interface of fluids is of paramount importance to understand and design new techniques and agents for IOR techniques, which can have a significant economic impact.

2. METHODOLOGY

All molecular dynamics calculations were performed by using the Large Atomic/Molecular Massively Parallel Simulator (LAMMPS) package. A critical ingredient in molecular dynamics simulations is the model of force field used to describe the systems. In our simulations, we have the H_2O molecules described as the SPCE/FH potential.[19] The force field consists of a 3-point charge model with inclusion of van der Waals and Coulomb interactions and flexible internal degrees of freedom. The internal degrees of freedom are taken into account by an O−H harmonic bond stretching and a H−O−H harmonic angle bending term. Na and Cl ions are described only by van der Waals and Coulomb terms. The parameters of the H_2O, Na, and Cl potentials are found in ref 19. Different salt concentrations have been considered: 0, 0.10, 0.25, 0.50, and 1%.

Carbon dioxide molecules were modeled using the flexible bonds potential,[20] which is based on the originally rigid EPM2 model. For N_2, we adopted the potential used in ref 21, and for CH_4, we adopted the potential contained in the CHARMM database.[22] For the crude oil model, we consider eight hydrocarbon types: alkanes [144 hexane (HEX), 132 heptane (HEP), 156 octane (OCT), 180 nonane (NON), 96 cyclohexane (CHEX), 156 cycloheptane (CHEP)] and aromatics [156 toluene (TOL) and 60 benzene (BEN)] molecules. Hydrocarbons were described using CHARMM-based force fields.[22]

The simulation cell for the isolated systems (H_2O (brine), CO_2, N_2, CH_4, and oil model) was set as a cubic box with dimensions $L_x \times L_y \times L_z$, where $L_x = L_y = L_z = 8.0$ nm. In total, 16 000 H_2O, 4000 CO_2, 4000 N_2, and 4000 CH_4 molecules were considered. A sequence of NVE (microcanonical ensemble), NVT (canonical ensemble), and NPT (isothermal−isobaric ensemble) calculations were performed to obtain the equilibrium densities for each of these fluids in pressures and temperatures ranging from 1 to 150 atm, and 300 to 350 K, respectively.

In this calculation protocol, for each system, we performed a 1.0 ps run in the NVE ensemble, a 10.0 ps run in the NVT ensemble, and a 2.0 ns run in the NPT ensemble. Periodic boundary conditions have been applied. For long-range electrostatic interactions, the reciprocal space particle particle particle-mesh (PPPM) method[23−25] was adopted. In all calculations, a time step of 0.5 fs and a cutoff of 10 Å was used for the van der Waals interactions. Temperature and pressure were controlled by a Nosé−Hoover thermostat and an Andersen barostat, respectively.

The oil−fluid interfaces were built considering the equilibrated isolated systems. The same protocol used for the pure fluids was repeated for the interfaced fluids. After equilibration, production MD runs were performed for 8 ns within the NVT ensemble. At this stage, the density profiles, interfacial tension between these systems, diffusion properties (self-diffusion and diffusion profile) were calculated.

To determine the interfacial tension, we consider a procedure based[20,23] on the formulation of the Gibbs interfacial tension as written in terms of pressures,

$$\gamma = \frac{1}{2}\int_{-L_b}^{L_a} \mathrm{d}z\,(p_{ab}(z) - p_T(z)) \tag{1}$$

where the distances L_a and $-L_b$ determine the limits of the interfacial region and $p_T(z)$ and $p_{ab}(z)$ are the tangential and normal components of the pressure tensor, respectively. We also calculate the interfacial tension profile,[23,26] which is defined as

$$\Delta\gamma^* = \left\langle \frac{p_{ab}(z) - p_T(z)}{2A} \right\rangle \tag{2}$$

where A is the area of a section in the xy-plane (parallel to interface). The pressure terms are calculated for each component in the atomic system and averaged over time with the Irving−Kirkwood theory.[23,26] For the per-atom virial calculation (pressure tensor), we follow the implementation within the LAMMPS code.[27] We also calculate the Gibbs adsorption isotherm,[28] where the surface excess of molecules can be written through

$$\Gamma_i = -\frac{1}{RT}\left(\frac{\partial\gamma}{\partial \ln C}\right)_{T,P} \tag{3}$$

where C is the salt concentration in solution, R is the gas constant, T is the temperature, P is the pressure, γ is the interfacial tension, and Γ_i is the isotherm.

The diffusion coefficients are calculated according to the Einstein relation,

$$D = \frac{1}{6}\lim_{t\to\infty}\frac{1}{N}\sum_{i=1}^{N}\frac{\mathrm{MSD}(t)}{t} \tag{4}$$

where D is the diffusion coefficient, $\mathrm{MSD}(t) = \langle (r_i(t) - r_i(0))^2 \rangle$ is the mean square displacement, and t is the time. To calculate

dx.doi.org/10.1021/jp310172j | J. Phys. Chem. B 2012, 116, 14667−14676

the diffusion profile, we consider the system divided into slabs of 5.0 Å thicknesses parallel to the interface.

To understand the effect of the fluid−oil interfaces on the orientation of the hydrocarbon chains, the angle between the vector connecting adjacent carbon atoms and the z axis (θ) was calculated as a function of the position (perpendicular to the interface) of the center of mass of pairs of carbon atoms. From this angle, the following order parameter was calculated.

$$S(\theta) = \frac{1}{2}(3\cos^2(\theta) - 1) \quad (5)$$

S will approach −1/2 when the molecule is parallel to the fluid/oil interface, 1.0 when the molecule is perpendicular to the interface, and 0.0 when there is no preferred orientation.

3. RESULT AND DISCUSSIONS

3.1. Density Profile and Interfacial Tension. Let us start our discussion by considering the case of the model of pure water in contact with oil. Figures 1 and 2 show the density profile along the direction perpendicular to the interface (z-axis) for the pure water/oil system at 300 and 350 K and 150 atm pressure, respectively. Here, the interface is determined by the Gibbs dividing surface (GDS),[29] which is defined as the location along the z-axis where the amount of excess H_2O molecules in the oil phase is approximately equal to the excess of oil molecules in the H_2O phase. The oil−fluid interface region (Δz^*) is determined considering the region within the GDS limits. The oil phase density profile can be visualized for the different hydrocarbon components within the oil mixture.

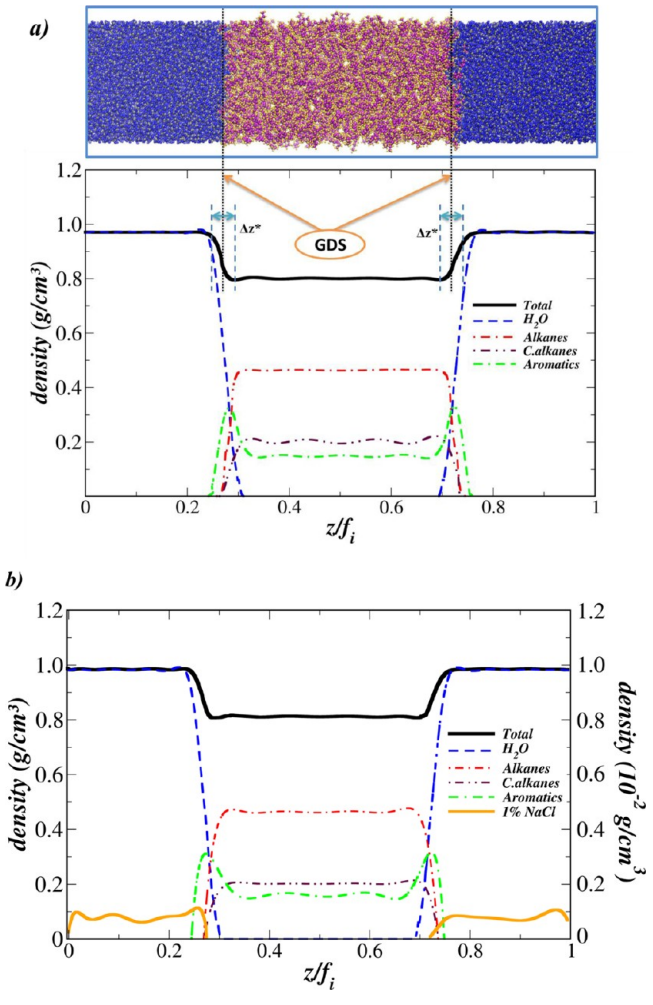

Figure 1. Density profile for the (a) H_2O/oil interface and (b) H_2O + (1%) NaCl/oil interface. All interfaces at 300 K and 150 atm. The green line shows an accumulation of aromatic molecules at the interfaces. Here z/f_i is a normalization factor of the box in the z direction, and f_i = 20 nm. In panel b, NaCl density can be seen only by applying a scaling factor; see the right axis.

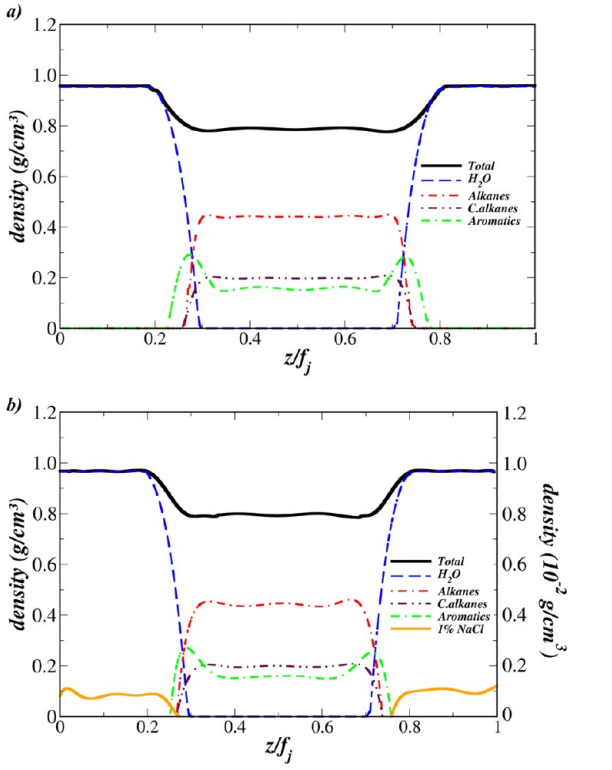

Figure 2. Density profile for the (a) H_2O/oil interface and (b) H_2O + (1%) NaCl/oil interface; all interfaces at 350 K and 150 atm. In green, we can see an accumulation of aromatic molecules at the interface. Here, z/f_i is a normalization factor of the box in the z direction, and f_i = 21.2 nm. In b, NaCl density can be seen only by applying a scaling factor; the see right axis.

In our calculations at 300 K and 150 atm, the density of pure H_2O was estimated to be 0.952 g/cm^3, which is in agreement with experimental values (0.944 g/cm^3).[30] For our oil model at the same conditions, the density was estimated to be 0.805 g/cm^3. Experimental results yield values that vary between 0.712 and 0.894 g/cm^3, according to the composition of the light oil model.[31]

From Figure 3, our simulations indicate that the density of aromatic molecules at the interface is about 2−3 times larger than the density of these molecules in the oil model (homogeneously distributed hydrocarbon mixture). This aromatic molecules accumulation effect at the interface was also reported in our recent work for a similar system (pure water/oil interface) but at higher pressures (400 atm).[31]

The explanation of this accumulation is related to the interfacial tension difference between aromatics−water and the other hydrocarbon−water (alkanes, cycloalkanes) interfaces.[30] The reason for this difference was suggested to be due to the weak hydrogen bonding between the aromatic rings and the water protons, which drives a lowering in the aromatics−water interfacial tension with respect to the other hydrocarbon systems.[31−35]

dx.doi.org/10.1021/jp310172j | J. Phys. Chem. B 2012, 116, 14667−14676

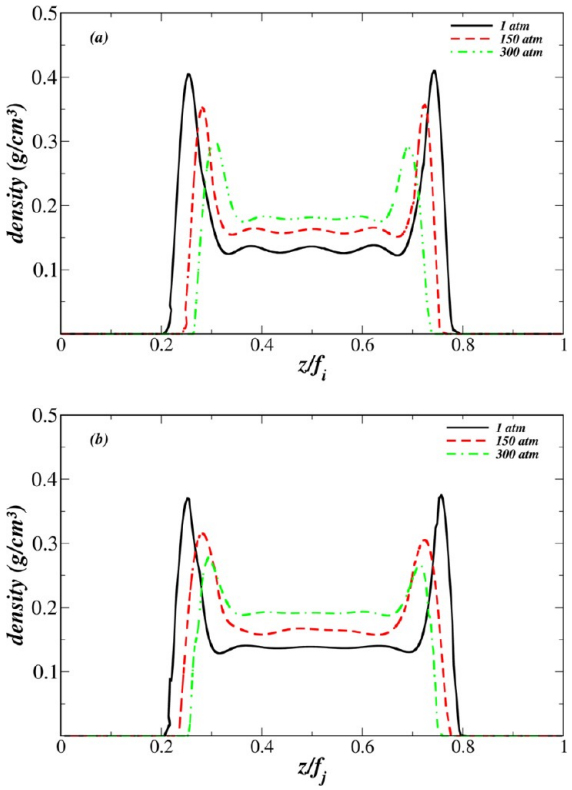

Figure 3. Density profile of aromatic molecules in a system containing a pure H_2O/oil interface at (a) 300 K and (b) 350 K and considered at only three pressures. Here, z/f_{ij} is a normalization factor of the box in the z direction, f_i = 22.0, 20.0, 19.0 nm, and f_j = 22.2, 21.2, 20.5 nm, calculated for each pressure, respectively.

Here, we extended ref 27 results to consider temperature, salt concentration and pressure effects. With increasing temperature (350 K) at the same pressure (150 atm), a decrease in the concentration of aromatic molecules is observed, as shown in Figures 2 and 3. To quantify the accumulation of aromatic molecules at a given temperature and pressure, we consider the ratio (d_{ac}) between the density of aromatic molecules in the oil–fluid interface region (Δz^*) with respect to the total density (d_t) of the same aromatic within the oil phase.

In Figure 4, we can see that for pure water, the aromatic accumulation in the interface decreases with increasing temperature and pressure. Instead, with increasing salt concentration at the same temperature and pressure, the accumulation of aromatic molecules at the interface does not vary significantly. This is consistent with the observation that the ions are uniformly distributed over the system and do not accumulate in the interface within the temperature, pressure, and salt concentration studied. The effect of the pressure is similar to that of the temperature, for which we observe a decrease in the aromatic molecules accumulation with increasing pressure. It is important to note that the H_2O (oil) density increases (decreases) with increasing pressure.

The interfacial tension as a function of pressure, temperature, and salt concentration is shown in Figure 5. The interfacial tension increases with increasing salt concentration (Figure 5a) and pressure (Figure 5b), and it decreases with increasing temperature (Figure 5a and b).[36−39] Our results are in agreement with experimental values for H_2O (pure)/octane (44 mN/m (1 atm and 298 K) to 54 mN/m (300 atm and 328K)).[40] Experimentally,[13] for crude oil/brine interfaces, it is

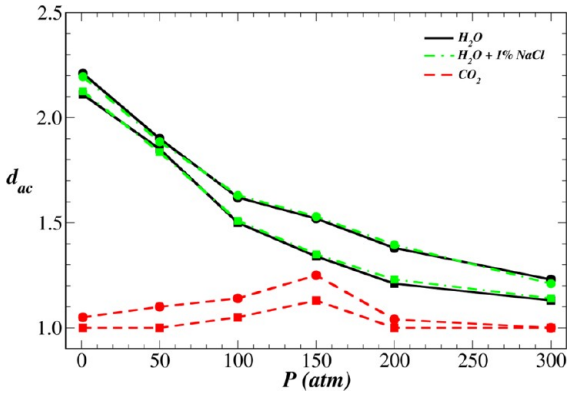

Figure 4. Density of aromatic accumulation d_{ac} for different temperatures and pressures. Here, H_2O/oil (pure and salt concentration of 1% NaCl) and CO_2/oil interfaces are shown. Circles, −300 K; squares, −350 K.

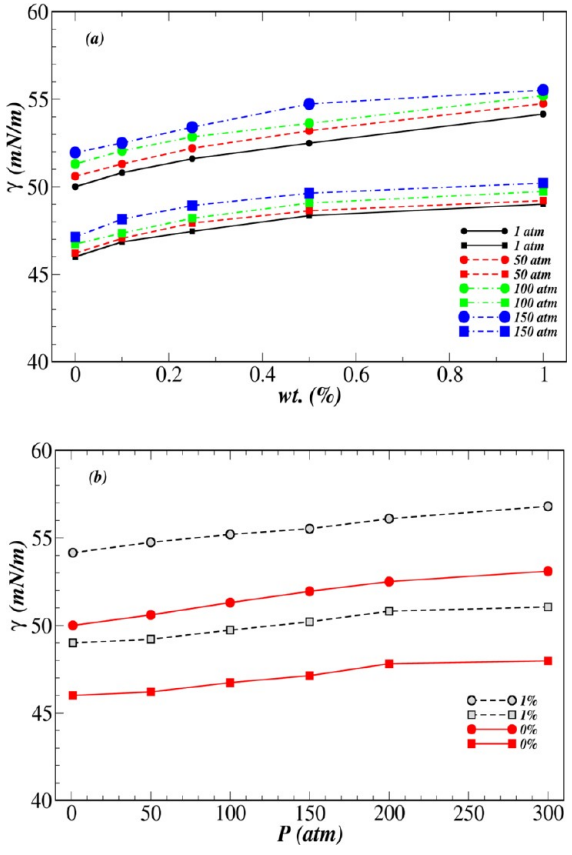

Figure 5. Interfacial tension for the H_2O + (%) NaCl/oil interface. (a) Interfacial tension depending on the salinity and different pressures and (b) interfacial tension depending on the pressure for two concentrations of NaCl. Circles, −300 K; squares, −350 K.

observed that the interfacial tension increases linearly with NaCl concentration. The effect of salinity for a given pressure causes a variation of 4−5 mN/m in brine/oil interfacial tension within the concentration studied.

On the basis of our interfacial tension results, we also calculate the Gibbs adsorption isotherm considering the salt concentration in the H_2O/oil interface (Figure 6), but no significant accumulation of ions at the interface region is observed. The magnitude of adsorption is close to 0.12 mol/m^2, at 1% NaCl and 350 K. The Gibbs adsorption isotherm is

dx.doi.org/10.1021/jp310172j | J. Phys. Chem. B 2012, 116, 14667−14676

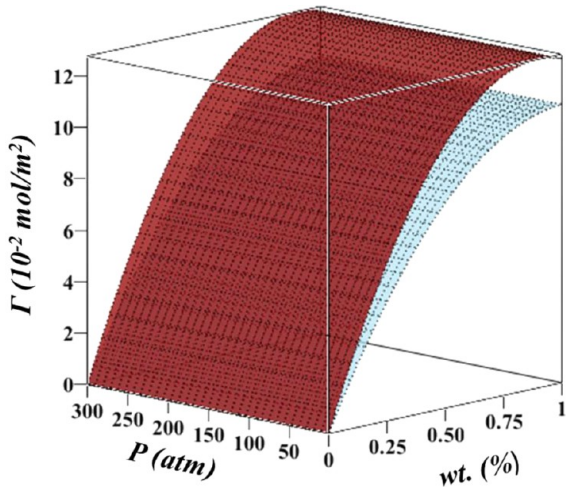

Figure 6. The surface excess of NaCl. Blue surface, −300 K; red surface −350 K. The functions that describe the curves are written as $\Gamma_T = (1/RT)C(5.2 - 2.54C)$, where C is salt concentration.

independent of the pressure and decreases with increasing temperature.

In what follows, we extend the same analysis as seen for brine/oil interfaces applied to other fluids studied here; namely, CO_2, N_2, and CH_4. Figure 7 displays the density profile for the

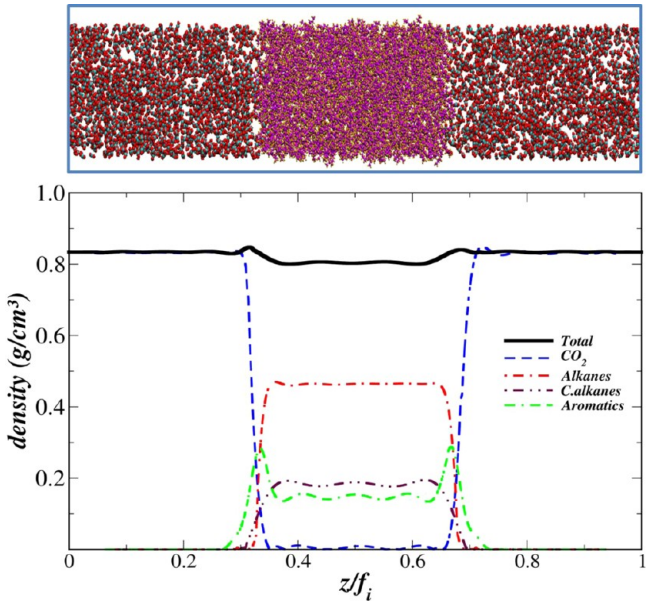

Figure 7. Density profile for the interface CO_2/oil at 300 K and 150 atm. In green, we can see an accumulation of aromatic molecules interface. Here, z/f_i is a normalization factor of the box in the z direction, and f_i = 22 nm.

system CO_2/oil at 300 K and 150 atm. Under the oil/CO_2 interface, the equilibrated density of CO_2 was found to be 0.841 g/cm^3, as compared with 0.843 g/cm^3 for pure CO_2. Experimental results show that the density is ∼0.849 g/cm^3 for pure CO_2.

An accumulation of aromatic molecules can be observed in the interfacial region similar to the brine/oil system (Figure 7). This suggests a stronger interaction of the CO_2 with the aromatic molecules in the interface compared with other hydrocarbons. In Figure 4, the accumulation density is also shown for CO_2. With increasing pressure, the aromatic density accumulation increases until 150 atm, regardless the temperature (300 and 350 K). This occurs even above 75 atm, where the CO_2 is already expected to be in the supercritical phase. At 150 atm, the CO_2 becomes miscible with the oil phase, and the CO_2/oil interface cannot be defined any longer. We also performed simulations of CO_2/oil interfaces at 400 K. At this temperature, the formation of an interface with the oil is not observed, even at low pressures (1−50 atm). In the literature,[13] a strong dependency of CO_2/oil miscibility on temperature is reported.

Figure 8 shows the density profile of the N_2/oil interfaces at 300 K and 150 atm. A slight accumulation of aromatic

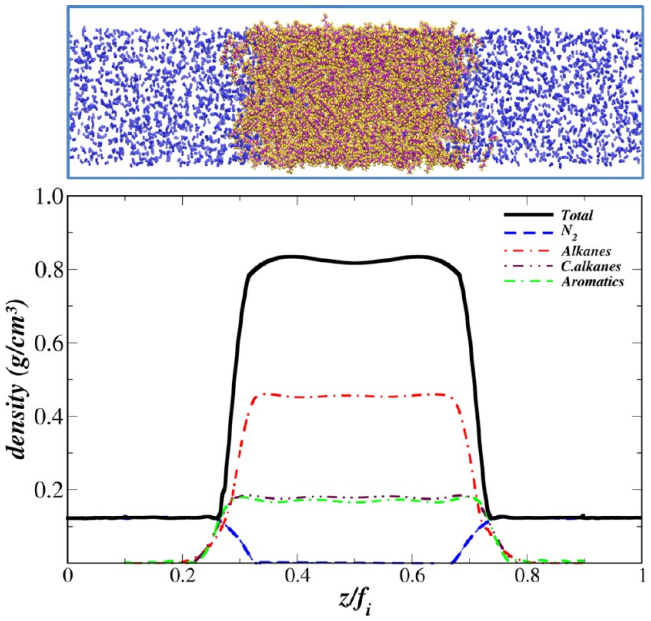

Figure 8. Density profile for the interface N_2/oil at 300 K and 150 atm. In green, we can see an accumulation of aromatic molecules interface. Here, z/f_i is a normalization factor of the box in the z direction, and f_i = 25 nm.

molecules can also be observed at the interfaces. A similar behavior is also observed for CH_4/oil interfaces. In Figure 9, a small accumulation of alkane molecules in addition to the aromatic molecules can be seen in the CH_4/oil interface. Our calculations suggest that for N_2/oil and CH_4/oil, no significant accumulation of aromatic molecules was observed with either temperature or pressure.

Figure 10 shows the interfacial tension profiles for the CO_2, N_2, and CH_4/oil systems at 300 K and 150 atm. In Table 1, we summarize the interface tension results from our MD calculations with the ones available experimentally. The effect of pressure and temperature on the interface tension can be observed in Figure 11, where regardless the fluid, the interfacial tension decreases with increasing pressure and temperature.

Put in context for all fluids studied, the calculated values for the interfacial tension of CO_2/oil are lower than the ones for H_2O/oil. The lower the interfacial tension, the more miscible the substances are. However, the values of the interfacial tension of N_2/oil were found to be higher than those for the CO_2/hydrocarbon interface, with a much less evident decrease with increasing pressure. This behavior can be explained as the result of the lower solubility of N_2 in a hydrocarbon mixture,

dx.doi.org/10.1021/jp310172j | J. Phys. Chem. B 2012, 116, 14667−14676

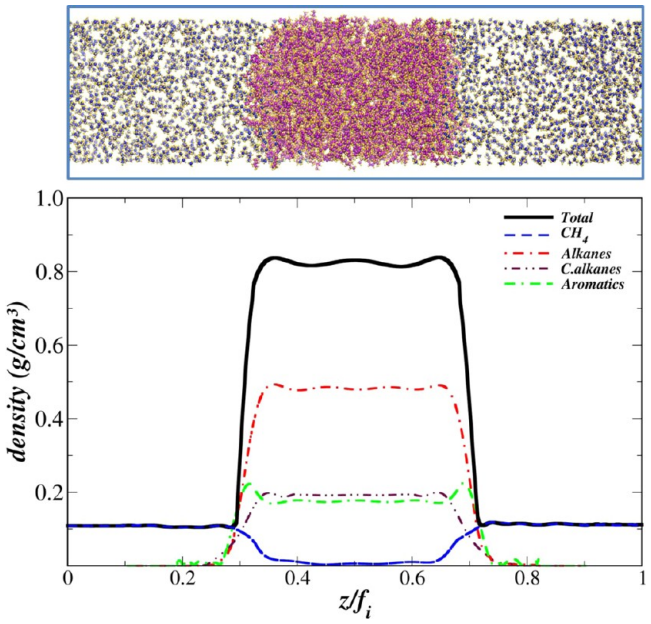

Figure 9. Density for the interface CH_4/oil at 300 K and 150 atm. In green, we can see an accumulation of aromatic molecules interface. Here, z/f_i is a normalization factor of the box in the z direction, and f_i = 25 nm.

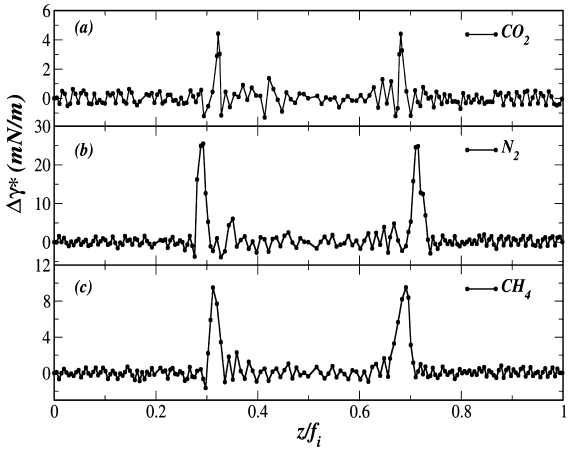

Figure 10. Interfacial tension profile for the fluids/oil interface at 300 K and 150 atm. Error estimate for the surface tension is calculated as 0.1 mN/m. Here, z/f_i is a normalization factor of the box in the z direction, and f_i = 22, 25, and 25 nm for the (a) CO_2, (b) N_2, and (c) CH_4 systems, respectively.

Table 1. Interfacial Tension in Fluid/Oil Interfaces at 300 K and 350 K and 150 atm

fluid in oil interface	γ (this work) (mN/m)	γ (exptl) (mN/m)
CO_2	4.5−2.7	22.0−1.0[41,a,42,a]
		23.0−1.0[43,b]
N_2	26.1−24.3	24.0[41,a]−13.0 [44,c]
CH_4	10.9−8.3	3.9[45,46,d]−7.8[41]

[a]In decane interface; pressure range: 1−200 atm at 300 K. [b]In crude oil interface; pressure range: 1−300 atm at 300 K and 331 K. [c]In octane interface; pressure: 300−400 atm; temperature: 373 K. [d]In heptane interface; pressure: 1−100 atm; temperature: 282 K.

with respect to that of CO_2, leading to a lower adsorption of N_2 at the interface. For the CH_4/oil interface, the interfacial

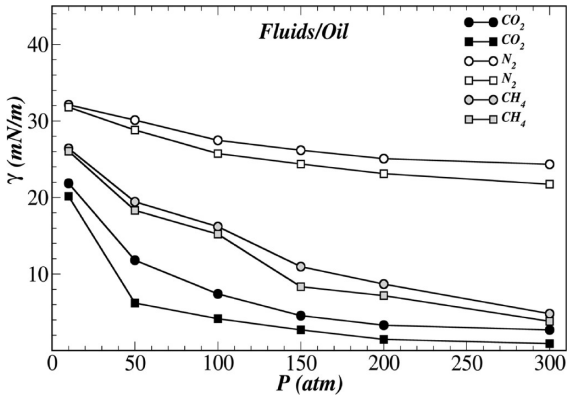

Figure 11. Fluids/oil surface tension at different pressures. Circle, −300 K and square, −350 K. Experimental values may be seen in refs 41−46.

tension values were comparable to the case of CO_2/oil, with a difference of ∼6 mN/m between the two interfaces. A lower value in the interfacial tension at the CH_4/oil interface means a higher miscibility of CH_4 in the oil phase.

3.2. Transport Properties for the (Brine and Fluid)/Oil Interfaces. Experimentally, it is very difficult to determine the diffusion coefficient for a given component in a multicomponent system. This is even more challenging for components that are chemically similar, such as a mixture of hydrocarbons. An advantage of molecular dynamics simulations is the possibility to directly determine the transport properties for each component within a complex chemical environment under different thermodynamic conditions.

Further exploring the thermodynamic properties of the interfaces studied here, in what follows, we will discuss the transport properties and the diffusion profiles along the fluid−oil interfaces. Initially, let us first determine the self-diffusion coeficients in a bulk system to then compare with the behavior of those systems at the interface. Figure 12 shows the calculated

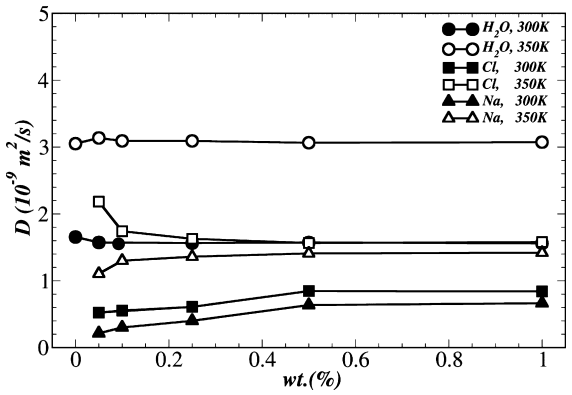

Figure 12. Diffusion coefficient for brine/oil interface at a pressure of 150 atm.

diffusion coefficients for brine as a function of salt concentration and temperature at 150 atm. Table 2 summarizes our calculated values for the fluids' diffusion coefficients in bulk and interfaced with oil. These results for brine and the other fluids are in agreement with both theoretical and experimental values.[19,47−52]

To understand the effect of the fluid−oil interface in the transport properties of the components, the variation of the

dx.doi.org/10.1021/jp310172j | J. Phys. Chem. B 2012, 116, 14667−14676

Table 2. Transport Properties in the Molecular Scale: Diffusion Coefficient in Fluid/Oil Interfaces at 300 K

fluid in oil interface	diffusion (this work) (10^{-9} m^2/s)	diffusion (exptl) (10^{-9} m^2/s)
CO_2	16.8	0.25[48,a]–11.6[49,50,b]
N_2	6.1	3.0–4.5[51,c]
CH_4	9.0	8.0[51,52]

[a]In heavy oil interface. [b]In decane interface. [c]In crude oil interface.

Table 3. f_i Values Relative to Figure 13 at 300 K

f_i in panel a (nm)	f_i in panel b (nm)	f_i in panel c (nm)	f_i in panel d (nm)	pressure (atm)
22.0	32.0	36.0	36.0	1
21.4	28.4	30.3	30.4	50
20.7	25.7	27.0	27.1	100
20.0	22.0	25.0	25.0	150
19.4	21.2	24.2	24.3	200
19.0	20.8	22.8	23.0	300

diffusion coefficient (along the direction perpendicular to the fluid/oil interfaces) was monitored as a function of pressure at 300 K (Figure 13). For all fluids considered, we observed a decrease in the diffusion coefficient toward the interface, regardless the pressure. These results suggests a decrease in the mobility at the fluid–oil interface.

For the brine/oil interface system, the effects of salinity on the diffusion profile were not significant when compared with the pure H_2O/oil case, even with increasing pressure. In general, the effect of salt is to modify the interfacial tension brine/oil interface. With increasing salt concentration, the solution is less miscible with oil, but the transport properties are not strongly affected compared with the pure water–oil interface. With increasing pressure, an increase in the fluid penetration on the oil phase is also observed. Moreover, the fluid concentration (CO_2, N_2, and CH_4) in the oil phase increases with pressure, which indicates a higher miscibility. The behavior observed in Figure 13b–d can be understood within the context of interfacial tension results due to the reduction in viscosity, density, and interfacial tension within the interface region.

For the CO_2/oil interface, we can verify the variation of CO_2 diffusivity in the oil phase for two distinct phases (gas and supercritical). In the gas phase (1–50 atm), CO_2 diffusion coefficient values are equivalent to those calculated for the other gases (N_2 and CH_4). However, a significant increase in the CO_2 diffusivity is observed at higher pressures, where CO_2 is in the supercritical regime.

Under reservoir conditions, the supercritical CO_2 was showed to be highly miscible in oil when compared with injection of other fluids (CH_4, N_2, and H_2O). This can be observed by its higher diffusion within the oil phase. Considering the diffusion profile for enzene and hexane, within our mixture oil model, the diffusion of these molecules in the interface region with pressure occurs in a manner similar to the injection of all fluids; that is, there is a decrease in the diffusion of the benzene and hexane molecules within the interface. For all cases, it can also be seen that there is an increase in the self-diffusion coefficients with increasing pressure for benzene molecules in the interface region. However, for the CH_4/oil interface, we observe only a slight increase in the self-diffusion coefficients for benzene and hexane in the interface region compared with other fluids.

3.3. Molecular Orientation. At the liquid–liquid interfaces, molecules may exhibit a preferential orientation because of the asymmetry in the forces experienced at the interface. This preferential orientation can be quantified on the basis of the orientation profile. This profile is the probability density $S(\theta)$ for the angle θ between some molecular axis (usually

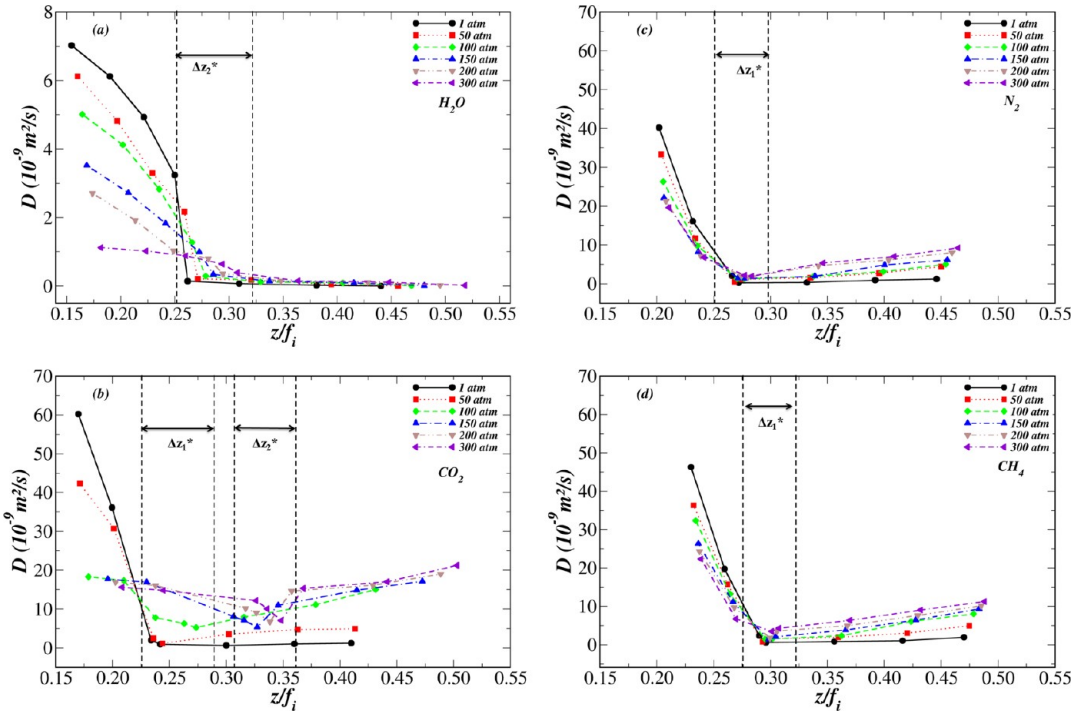

Figure 13. Diffusion profile for all fluid/oil systems. The range Δz_1^*(gas/oil interface) and Δz_2^*(liquid/oil interface) are determined considering the region within the GDS limits, at 300 K. (a) H_2O/oil, (b) CO_2/oil, (c) N_2/oil, (d) CH_4/oil. The factor f_i scales can be seen in Table 3.

dx.doi.org/10.1021/jp310172j | J. Phys. Chem. B 2012, 116, 14667–14676

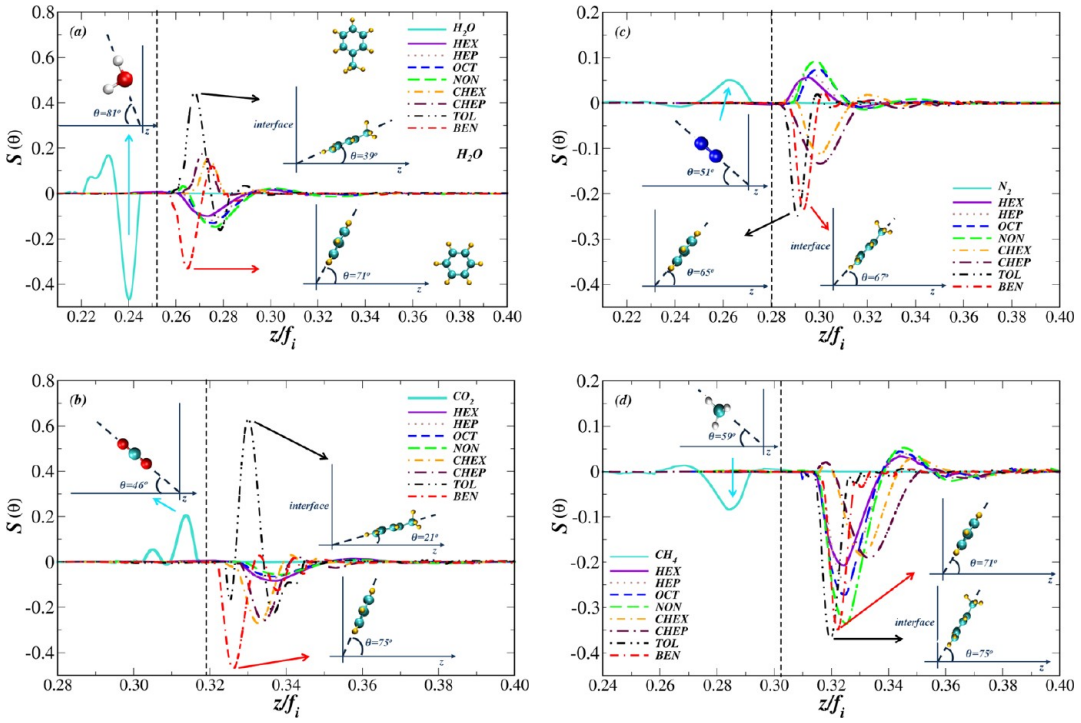

Figure 14. Profile of average orientational order from the angle of the vector between adjacent carbons and the z axis as a function of atomic position. Dotted line represents the GDS (Gibbs dividing surface). (a) H_2O, (b) CO_2, (c) N_2, and (d) CH_4 systems at 300 K and 150 atm. All panels have the representation of the orientation of benzene and toluene molecules relative to the interface.

coinciding with the direction of the molecule electric dipole moment) and the normal to the interface for different locations z along the interface normal.

Figure 14 displays the time-averaged order parameter $S(\theta)$ for each hydrocarbon considered in our oil model at 300 K and 150 atm. At the H_2O/oil interface (Figure 14a), there is a preferential orientation of the aromatic molecules in the interface region (between 0.26 and 0.29 z/f_i units; here, z/f_i is a normalization factor of the box in the z direction). The first $S(\theta)$ peak indicates a tilted angle with respect to the interface of 71° (39°) for benzene (toluene). For alkanes, our calculation suggests an increase in the order parameter with increasing chain length. The average angle for alkanes was found to be between 56° and 60°, whereas for cycloalkanes, this average angle ranges between 49° and 50°.

For the CO_2/oil interface, Figure 14b indicates a similar orientational behavior for alkanes with respect to the H_2O/oil interface. However, larger angles (~63°) were observed for cycloalkanes. On the other hand, this angle slightly increases for benzene (75°), but it shows a considerable decrease (21°) in the toluene preferential angle orientation. In the case of the N_2/oil interface (Figure 14c), the angular orientation for alkanes was found to be between 46° and 50° with respect to the interface, it is similarly observed for benzene and toluene (~65°), although for the cycloalkanes, the angular orientation was found to be 57° and 61°. For the CH_4/oil interface (Figure 14d), the angular orientation for aromatics was found to have similar values for two molecules: benzene (71°) and toluene (75°). In addition, larger angles ranging between the alkane molecules (i.e., the angle range between 62° and 75°) were observed with increasing chain length. For cycloalkanes, for both molecules studied, the values have similar angular orientation (~62°).

For all the fluids studied, the system tends to become more disorganized in the interfacial region with increasing temperature (not shown). On the other hand, with increasing pressure, the aromatic molecules tend to have the aromatic ring parallel in the H_2O/oil system interface (80° for benzene at 300 K and 300 atm). However, for the CO_2/oil interface, an opposite situation was found. There is no preferential orientation of hydrocarbon molecules relative to the interface because of the increased miscibility of CO_2 with increasing pressure. A similar effect also occurs for the CH_4/oil interface. In the case of the N_2/oil interface, there is a gradual decrease in the hydrocarbon orientational order parameter in the interface region due to increased diffusion of N_2 molecules in the oil phase, but this effect is not evident in the CH_4 case.

The angular orientation for the injected fluids with respect to the interface was also obtained. For H_2O, an angle of 81° was found, which indicates the orientation of the O atoms toward the interface region. In the case of CO_2, a angle of 46° was observed and, similarly to the case of H_2O, the molecule points out directly to the interface region. For N_2 and CH_4 molecules, the angles obtained were of 51° and 59°, respectively. The difference between the fluid H_2O and CO_2 with respect to N_2 and CH_4 is evidenced by the presence of orientation peaks in the graphs of Figure 14. At 300 K and 150 atm, H_2O and CO_2 are in the liquid and the supercritical phases, respectively, and two well-pronounced peaks are observed on their orientational order parameter. Instead, for the gaseous fluids (CH_4 and N_2) under the same conditions, a very sharp peak is observed.

Putting the results in perspective, for the CO_2, N_2, and CH_4 fluids, the simulations suggest a decrease in the interfacial tension and an increase in the fluid diffusion in the oil phase with increasing pressure, followed by a decrease in the molecular preferential orientation for both components (fluid−oil). In a nutshell, for those systems, the lower the

dx.doi.org/10.1021/jp310172j | J. Phys. Chem. B 2012, 116, 14667−14676

interfacial tension, the lower the orientation of molecules in the interface region will be and the larger the penetration of the fluid in the oil phase. On the other hand, for the brine/oil interface, our calculations indicate an increase in the interfacial tension with increasing pressure and salt concentration. However, the H_2O self-diffusion coefficient decreases with increasing salt concentration. There is no substantial variation in the H_2O molecule orientation within the interface with increasing pressure. A similar effect is observed with the interface tension, which does not vary significantly with molecule disordering within the interface. The combination of these results on the diffusion coefficients, interfacial tension, and molecular orientation suggests that the brine/oil components are immiscible under the temperature and pressure range studied.

4. CONCLUSION

The structural and dynamic properties of typical injected IOR fluid−oil interfaces have been investigated from molecular dynamics simulations under different conditions of temperature, pressure, and salt concentration. Interestingly, we have studied the accumulation of aromatic molecules within the brine/oil and fluid/oil interfaces. This accumulation was observed for both brine and CO_2 interfaces, and it decreases with increasing temperature and pressure. The accumulation was not observed at high reservoir temperatures (400 K), regardless the fluid studied. The formation of a layered interface rich with aromatic molecules may be a critical factor in determining the interfacial behavior for IOR technologies.

For a brine/oil interface, an increasing in the interfacial tension was observed with increasing pressure and salt concentration. In the aqueous solution, the effect of water molecules hydration on the ions leads to an increase in the immiscibility between oil and brine in the interface within the salt concentration studied. However, for the other fluids, our calculations indicate a decrease in the interfacial tension with increasing pressure. Particularly for CO_2 and methane above 150 atm, this decrease in the interfacial tension is such that it leads to miscibility between the components (fluid and oil). In the case of N_2, this effect is not observed, since this decrease is not pronounced, as compared with CO_2 and methane.

The effect of the interface on the transport properties was analyzed by determining the diffusion coefficient profile from the bulk toward the interface region. This is particularly important to correlate the effects of interface tension and diffusion profiles on the miscibility between the interface components. For a pure water−oil interface, water molecule diffusion within the oil phase was not observed; however, in the interface region, we observed a slight increase in the mobility with increasing pressure. For a given temperature, with increasing pressure, there is an increase in the diffusion coefficients of injected fluids within the oil phase. For CO_2, these values are significantly higher than the other fluids. Concomitantly with the lower interfacial tension values, our calculations also suggest a complete miscibility between the components above 150 atm for the cases of CO_2 and methane. Variations on molecular orientation between fluid−oil components in the interface region were correlated to the interfacial tension and diffusivity with the increased pressure and temperature. Interestingly, a nonpreferential molecular orientation was observed with increasing fluid miscibility with oil.

From a molecular perspective of fluid−oil interfaces for IOR applications, the main contributions of this paper can be summarized as follows:

1. The brine/oil interfacial properties indicate that an increase in the salt concentration and pressure leads to an increase in the interfacial tension. This effect favors the displacement of oil because of the enhancement of the mechanical contact between the fluids.
2. For nitrogen gas, the combination of slower diffusion with higher interfacial tension values compared with other injected fluids and no aromatic molecular accumulation in the interface suggests this fluid may be an interesting one to maintain the thermodynamic reservoir properties, such as the pressure.
3. The combined methane−oil interface properties of miscibility, increasing the diffusion of CH_4 molecules within the oil phase with increasing pressure followed by the decrease in the interfacial tension makes methane an excellent fluid for IOR applications as a secondary fluid injection since this gas is also found naturally in reservoirs.
4. Finally, for the study of the gas/liquid CO_2, this fluid has proved the most effective among all other fluids studied. Our calculations indicate that the miscibility of CO_2 increases with increasing pressure. In its supercritical phase, interfacial tension values become so small that in some cases (T = 400 K), its calculation is not possible because the CO_2−oil interface can no longer be defined. The combination of low interfacial tension with high CO_2 diffusion in the oil phase gives CO_2 unique physical chemistry properties for IOR applications.

AUTHOR INFORMATION

Corresponding Author

*E-mail: caetano.miranda@ufabc.edu.br.

Notes

The authors declare no competing financial interest.

ACKNOWLEDGMENTS

We acknowledge financial support from the Brazilian agencies FAPESP, CAPES, and CNPq and Dr. Y. Liang for valuable comments. The calculations were partially performed at CENAPAD-SP, CESUP-RS, and UFABC supercomputer facilities.

REFERENCES

(1) Petersen, K. S.; Christensen, P. L. *Phase Behavior of Petroleum Reservoir Fluids*, CRC Press, Boca Raton, FL, 2007, pp 81−112.
(2) Navrotsky, A. *Nat. Mater.* **2003**, *2*, 571−572.
(3) Biben, T.; Joly, L. *Phys. Rev. Lett.* **2008**, *100*, 186103−186106.
(4) Buckley, J. S.; Fan, T. *Petrophysics* **2007**, *48*, 175−185.
(5) Benjamin, I. *Annu. Rev. Phys. Chem.* **1997**, *48*, 407−451.
(6) Jungwirth, P.; Finlayson-Pitts, B. J.; Tobias, D. *J. Chem. Rev.* **2006**, *106*, 1137−1139.
(7) Chandler, D. *Nature* **2007**, *445*, 831−832.
(8) Hore, D. K.; Walker, D. S.; Richmond, G. L. *J. Am. Chem. Soc.* **2008**, *130*, 1800−1801.
(9) Bonn, D.; Eggers, J.; Indekeu, J.; Meunier, J.; Rolley, E. *Rev. Mod. Phys.* **2009**, *81*, 739−805.
(10) Mitrinovic, D. M.; Tikhonov, A. M.; Li, M.; Huang, Z.; Schlossman, M. L. *Phys. Rev. Lett.* **2000**, *85*, 582−585.
(11) Du, Q.; Freysz, E.; Shen, Y. R. *Science* **1994**, *264*, 826−828.

(12) Scatena, L. F.; Brown, M. G.; Richmond, G. L. *Science* **2001**, *292*, 908−912.
(13) De Serio, M.; Mohapatra, H.; Zenobi, R.; Deckert, V. *Chem. Phys. Lett.* **2006**, *417*, 452−456.
(14) Nomoto, T.; Onishi, H. *Phys. Chem. Chem. Phys.* **2007**, *9*, 5515−5521.
(15) Lambert, J.; Hergenröder, R.; Suter, D.; Deckert, V. *Angew. Chem., Int. Ed.* **2009**, *48*, 6343−6345.
(16) Trivedi, J. J.; Babadagli, T. *SPE117607*; SPE Eastern Regional/AAPG Eastern Section Joint Meeting, 11−15 October 2008, Pittsburgh, Pennsylvania; Society of Petroleum Engineers: Allen, TX
(17) Godec, M.; Kuuskraa, V.; Van Leeuwen, V.; Melzer, L. S.; Wildgust, N. *Energy Procedia* **2011**, *4*, 2162−2169.
(18) Farajzadeh, R.; Andrianov, A.; Zitha, P. L. J. *Ind. Eng. Chem. Res.* **2010**, *49*, 1910−1919.
(19) Alejandre, J.; Chapela, G. A.; Bresme, F.; Hansen, J.-P. *J. Chem. Phys.* **2009**, *130*, 174505−174514.
(20) Nieto-Draghi, C.; de Bruin, T.; Perez-Pellitero, J.; Avalos, J. B.; Mackie, A. D. *J. Chem. Phys.* **2007**, *126*, 064509−064516.
(21) Sokhan, V. P.; Nicholson, D. *J. Chem. Phys.* **2004**, *120*, 3855−3864.
(22) Brooks, B. R. *J. Comput. Chem.* **2009**, *30*, 1545−1615.
(23) Jang, S. S.; Lin, S.-T.; Maiti, P. K.; Blanco, M.; Goddard, W. A. J.; Shuler, P.; Tang, Y. *J. Phys. Chem. B* **2004**, *108*, 12130−12140.
(24) Hockney, R. W.; Eastwood, J. W. *Computer Simulation Using Particles*; Adam Hilger, Philadelphia, 1989.
(25) Thompson, A. P.; Plimpton, S. J.; Mattson, W. *J. Chem. Phys.* **2009**, *131*, 154107−154112.
(26) Ghoufi, A.; Goujon, F.; Lachet, V.; Malfreyt, P. *J. Chem. Phys.* **2008**, *128*, 154716−154731.
(27) Plimpton, S. J. *J. Comput. Phys.* **1995**, *117*, 1−19.
(28) Gurkov, T. D.; Dimitrova, D. T.; Marinova, K. G.; Bilke-Crause, C.; Gerber, C.; Ivanov, I. B. *Colloids Surf., A* **2005**, *261*, 29−38.
(29) Chattoraj, D. K.; Birdi, K. S. *Adsorption and the Gibbs Surface Excess*; Plenum Publishing Company: New York, 1984. Talu, O.; Myers, A. L. *AIChE J.* **2001**, *47*, 1160−1168.
(30) Ueno, M.; Mitsui, R.; Iwahashi, H.; Tsuchihashi, N.; Ibuki, K. *J. Phys.: Conf. Ser.* **2010**, *215*, 012074.
(31) Kunieda, M.; Nakaoka, K.; Liang, Y.; Miranda, C. R.; Ueda, A.; Takahashi, S.; Okabe, H.; Matsuoka, T. *J. Am. Chem. Soc.* **2010**, *132*, 18281−18286.
(32) Fernandes, P. A.; Cordeiro, N. D. S.; Gomes, J. A. N. F. *J. Phys. Chem. B* **1999**, *103*, 6290−6299.
(33) Jedlovszky, P.; Varga, I.; Gilányi, T. *J. Chem. Phys.* **2003**, *119*, 1731−1740.
(34) Franks, H. S.; Evans, M. *J. Chem. Phys.* **1945**, *13*, 507−532.
(35) Dang, L. X.; Feller, D. *J. Phys. Chem. B* **2000**, *104*, 4403−4407.
(36) Eley, D. D. *Trans. Faraday Soc.* **1939**, *35*, 1281−1293.
(37) Massoudi, R.; King, A. D. *J. Chem. Phys.* **1975**, *79*, 1676−1679.
(38) Chiang, M. Y.; Chan, K. S.; Shah, D. O. *J. Can. Pet. Technol.* **1978**, *17*, 4−9.
(39) Fall, A.; Rimstidt, J. D.; Bodnar, R. J. *Am. Mineral.* **2009**, *94*, 1569−1579.
(40) Al-Sahhaf, T.; Elkamel, A.; Suttar Ahmed, A.; Khan, A. R. *Chem. Eng. Commun.* **2005**, *192*, 667−684.
(41) Miqueu, C.; Mendiboure, B.; Gracia, C.; Lachaise, J. *Fluid Phase Equilib.* **2004**, *218*, 189−203.
(42) Sahimi, M.; Taylor, B. N. *J. Chem. Phys.* **1991**, *95*, 6749−6761.
(43) Yang, D.; Gu, Y. *Pet. Sci. Technol.* **2005**, *23* (9−10), 1099−1112.
(44) Huygens, R. J. M.; Ronde, H.; Hagoort, J. *SPE J.* **1993**, SPE26643.
(45) Amin, R.; Smith, T. N. *Fluid Phase Equilib.* **1998**, *142*, 231−241.
(46) Peng, B.-Z.; Sun, C.-Y.; Liu, B.; Zhang, Q.; Chen, J.; Li, W.-Z.; Chen, G.-J. *J. Chem. Eng. Data* **2011**, *56*, 4623−4626.
(47) Lara, L. S.; Michelon, M. F.; Metin, C. O.; Nguyen, Q. P.; Miranda, C. R. unpublished results.
(48) Tharanivasan, A. K.; Yang, C.; Gu, Y. *Energy Fuels* **2006**, *20*, 2509−2517.
(49) Dysthe, D. K.; Fuchs, A. H.; Rousseau, B. *Int. J. Thermophys.* **1998**, *19*, 437−448.
(50) Zabala, D.; Nieto-Draghi, C.; Hemptinne, J. C.; Ramos, A. L. L. *J. Phys. Chem. B* **2008**, *112* (51), 16610−16618.
(51) Riazi, M. R.; Whitson, C. H. *Ind. Eng. Chem. Res.* **1993**, *32*, 3081−3088.
(52) Jamialahmadi, M.; Emadi, M.; Müller-Steinhagen, H. *J. Pet. Sci. Eng.* **2006**, *53*, 47−60.